The Potential of Heat Transfer Control on Insulated Combustion Chamber Walls

K.Nishiwaki and T.Hagiwara

Department of Mechanical Engineering
Ritsumeikan University
56-1 Toji-in Kitamachi
Kita-ku, Kyoto 603
Japan

ABSTRACT

Detailed heat transfer analyses were made including heat release in an unsteady turbulent thermal boundary layer with emphasis on the surface heat fluxes at elevated wall temperatures ranging up to 1100 K. The one-dimensional numerical studies have given a possible answer to the question whether the heat flux increases or decreases during combustion by the use of ceramics for combustion chamber walls in reciprocating i.c. engines. The results indicate that when the gas motion is induced only by compression or expansion, the heat flux increases with increasing wall temperature because the quench distance becomes shorter. It is also indicated that when there is an additional gas motion approaching the wall, which implies the penetration into a porous wall or the wall-impingement of a fuel spray, the heat flux decreases with increasing wall temperature due to non-reactive hot combustion products coming close to the wall. It is suggested that only a little additional gas motion is enough to exert a significant effect.

INTRODUCTION

Adiabatic or insulated diesel engines are being developed with the expectation of reducing heat losses by using ceramics or heat resistant metals as combustion chamber wall materials. However, several experimental results have posed the problem that higher wall temperatures result in higher surface heat fluxes during a combustion period, being inconsistent with the well-known behavior of thermal boundary layers. Such results have been shown by Furuhama and Enomoto[1], Woschni et al.[2,3], and Huang and Borman[4]. On the other hand, there have been nearly the same number of experiments which have shown that the surface heat fluxes during a combustion period decrease in the insulated engines as expected. These results are seen in the works presented by Furuhama and Enomoto(1), Huang and Borman(4), Morel et al.(5), and Chen et al.(6).

With regards to steady combustion systems, Germerdonk and Nguyen(7) showed that the heat transfer coefficient abruptly increases at wall temperatures of higher than 873 K on the wall of a furnace using a propane-air diffusion flame. They also introduced the experimental results obtained by using an wall-impinging jet flame, but the data did not show any significant change in the heat transfer coefficient at different wall temperatures.

There has been no answer given to the contradiction between these results, although extensive discussions were done by several researchers in the Ref. 3.

From a theoretical point of view, all the heat transfer models for i. c. engine processes did not take heat release into consideration except the one-dimensional model due to Yang and Martin(8) which was recently presented. However, the model did not include temperature-dependent combustion reactions. The results indicated that in most cases of the parametric study lower wall temperatures resulted in higher heat transfer.

The present work aims at finding the reason or in what case heat fluxes increase or decrease as the wall temperature is elevated. One-dimensional models were numerically solved for a reactive turbulent thermal boundary layer, giving a possible answer to the problem.

FORMULATION OF THE ONE-DIMENSIONAL MODEL FOR UNSTEADY REACTIVE TURBULENT THERMAL BOUNDARY LAYER

The system to be solved is a combustion chamber of a reciprocating engine having a flat cylinder head. The governing differential equations are described in a one-dimensional coordinate perpendicular to the cylinder head with the ensemble-averaged dependent variables which include: velocity u, enthalpy h, turbulent kinetic energy k, dissipation rate ε, and mass fractions m_{fu}, m_{ox} and m_{pr} of fuel, oxygen and combustion products, respectively. By introducing uniform-pressure assumption, every equation can be represented by the following general conservation equation with ψ standing for each dependent variable:

$$\frac{\partial}{\partial t}(\rho\psi) + \frac{\partial}{\partial x}(\rho u\psi) = \frac{\partial}{\partial x}\left(\Gamma_\psi \frac{\partial \psi}{\partial x}\right) + S_\psi \quad (1)$$

where ρ is the density; Γ_ψ and S_ψ denote the corresponding effective viscosity and source term, respectively, the definitions of which are shown in Table 1.

The turbulent viscosity μ_t is given by

$$\mu_t = C_\mu f_\mu \frac{\rho k^2}{\varepsilon} \quad (2)$$

Table 1 Definitions of ψ, $\Gamma\psi$, and $S\psi$

ψ	$\Gamma\psi$	$S\psi$
1	0	0
h	$\frac{\mu}{Pr}+\frac{\mu_t}{Pr_t}$	$\frac{dp}{dt}+Hu\cdot R_f$
k	$\frac{\mu_t}{\sigma_k}$	$\mu_t\{(\frac{\partial v}{\partial x})^2+2(\frac{\partial u}{\partial x})^2\}-\frac{2}{3}\frac{\partial u}{\partial x}(\mu_t\frac{\partial u}{\partial x}+\rho k)-\rho\varepsilon$
ε	$\frac{\mu_t}{\sigma_\varepsilon}$	$\frac{\varepsilon}{k}f_1[C_1\mu_t\{(\frac{\partial v}{\partial x})^2+2(\frac{\partial u}{\partial x})^2\}-\frac{2}{3}\frac{\partial u}{\partial x}(C_1'\mu_t\frac{\partial u}{\partial x}+C_1''\rho k)]-C_2f_2\rho\frac{\varepsilon^2}{k}+C_3\rho\varepsilon\frac{\partial u}{\partial x}$
m_{fu}	$\frac{D}{S_c}+\frac{\mu_t}{\sigma_m}$	$-R_f$
m_{ox}	$\frac{D}{S_c}+\frac{\mu_t}{\sigma_m}$	$-S\cdot R_f$
m_{or}	$\frac{D}{S_c}+\frac{\mu_t}{\sigma_m}$	$(S+1)\cdot R_f$

D:diffusion coefficient
Hu:lower heating value
p:pressure
Pr:Prandtl number
Pr_t:turbulent Prandtl number=1
R_f:heat release rate
S:stoichometric combination ratio
Sc:Schmidt number
μ:molecular viscosity
μ_t:turbulent viscosity

Table 2 Model coefficients and model functions used in the k-ε model

σ_k	1.0	C_1	1.44	C_2	1.92
σ_ε	1.3	C_1'	1.32	C_3	1.0
σ_m	1.0	C_1''	4.50	C_μ	0.09

$f_1=1.0$

$f_2=[1-\frac{2}{9}\exp\{-(\frac{R_t}{6})^2\}]\{1-\exp(-\frac{y^+}{5})\}^2$

$f_\mu=(1+\frac{3.45}{\sqrt{R_t}})\{1-\exp(-\frac{y^+}{70})\}$

$R_t=\frac{k^2}{\nu\varepsilon}$, $y^+=\frac{u_\tau x}{\nu}$,

u_τ:friction velocity, ν:kinematic viscosity

where C_μ is an empirical coefficient and f_μ is a model function. Table 2 indicates the values of coefficient C_μ and other coefficients appearing in Table 1. The model function f_μ and other model functions used in the k-ε model are also given in Table 2.

The k-ε model used in the present analyses is produced by combining the model coefficients which includes the compression effect adapted from Morel-Monsour's work(9), and the model functions proposed by Myong-Kasagi(10) to describe a continuous change in turbulent characteristics from a low Reynolds number region (near the wall) to a high Reynolds number region (far from the wall). The continuous representation of turbulent characteristics is indispensable to the heat release model in the present analyses.

The velocity component, u, perpendicular to the wall is solved by way of the continuity equation. The velocity component, v, parallel to the wall is taken into account to integrate swirling flow effects on turbulence. This velocity is assumed to obey the logarithmic law of the wall with an assumed velocity outside the boundary layer, which is set the mean piston speed at B.D.C. and then decreases in a linear time-change to 60 % of the initial value at T.D.C.

The heat release model is represented by the combination of the eddy-break-up model and the Arrhenius-type model for a one-step global reaction, which was employed by Gosman and Harvey-(11). The idea of the model is that the time scales characterized by turbulent mixing and chemical reaction are compared and then the longer one is taken as a controlling time scale.

The characteristic time scale τ_m and burning rate R_f for turbulent mixing are given by Eqs. (3) and (4),respectively.

$$\tau_m=\frac{k}{\varepsilon} \tag{3}$$

$$R_f=A\rho\frac{1}{\tau_m}MIN[m_{fu},\frac{m_{ox}}{S},\frac{Bm_{or}}{1+S}] \tag{4}$$

where MIN denotes a function which takes the minimum; A and B are empirical coefficients and assumed 20 and 0.5, respectively.

For the chemical reaction, the characteristic time scale τ_r and the burning rate R_f are written as follows:

$$\tau_r=\frac{1}{C\rho\exp(-D/T)} \tag{5}$$

$$R_f=\frac{\rho m_{fu}m_{ox}}{\tau_r} \tag{6}$$

where C is an empirical coefficient and D the activation temperature, both of which depend on a fuel. In the present computations, propane is used as a fuel to evaluate C and D. Dissociation was not taken into account, because it was found insignificant in preliminary computations as far as the wall heat flux is concerned. The molecular viscosity and specific heats are assumed to be functions of temperature.

The governing equations are solved in the half of the range between the cylinder head and piston with x=0 at the cylinder head and x=L in the middle. The fuel distribution is given at the time of ignition (-25deg. CA) which takes place at x=L; L=4 mm at -25 deg. CA. Before the ignition, only an air exists in the combustion chamber.

The model describes a simplified local combustion process in which the fuel injection takes place followed by the ignition and then a

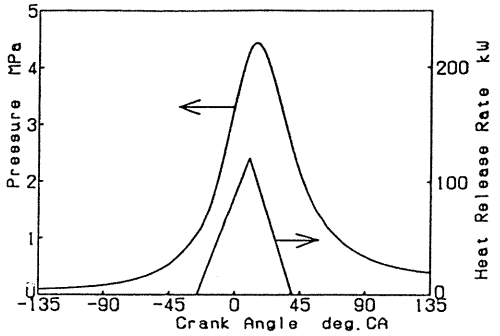

Fig. 1 Pressure-time curve given by assumed global heat release rate

flame propagates to the wall. This does not mean the model represents the whole combustion process in the combustion chamber. From this point of view, a heat release rate in the whole combustion chamber is independently given and thus the pressure is calculated by a global thermodynamic model or one-zone model.

Radiation heat transfer is not considered. The data of Oguri and Inaba(12) showed that the peak value of radiation heat flux is 15 % of that of the total heat flux in a d. i. diesel. In this view, the problem under consideration is thought to be mostly involved in convection heat transfer.

The engine used for the present study has a bore of 80 mm, a stroke of 80 mm and a compression ratio of 9. The engine speed was set to be 1000 rpm.

Figure 1 shows a pressure-time curve calculated with an assumed global heat release rate. The same pressure-time curve was used in every case of the present study.

The wall temperatures were selected between 300 K and 1100 K. The wall temperature of 1100 K is almost the maximum value which has been attained in ceramic engines.

An implicit method numerically solved a set of the governing equations with a grid spacing of 30 microns in the region within 3 mm from the wall and 60 microns beyond it. Each computation started at -135 deg. CA with the initial gas temperature of 320 K and the initial pressure of 0.1013 MPa, and terminated 135 deg. CA.

HEAT FLUXES FOR DIFFERENT FUEL DISTRIBUTIONS

Computations were carried out at several different high wall temperatures, assumed constant, for the three different spatial distributions of fuel-air mixture given in the following:

A. A uniform distribution with an equivalence ratio ϕ=1.0.
B. A non-uniform distribution with ϕ=0 at the wall and ϕ=2.0 at x=L, having a linear distribution in between; L=4 mm
C. A non-uniform distribution with ϕ=0.5 at the wall and ϕ=1.5 at x=L, having a linear distribution in between.

Figure 2 shows wall heat fluxes computed at several different wall temperatures for the fuel distribution A. It is seen that during compression the heat flux decreases with increasing wall temperature . This is a well-known tendency seen in non-reacting thermal boundary layers.

On the other hand, it is noted that the heat flux peaks higher with increasing wall temperature during combustion; this is a reversal of the well-known tendency. The reason for this is explained by the fact that a quench distance becomes shorter as the wall temperature increases, as is shown in Fig. 3; the quench distance was obtained by finding the distance where the 1500 K point of gas temperature comes closest to the wall. In the temperature distributions which were measured by Lucht et. al(11) with the CARS method in an s.i. engine having the same compression ratio and using the same fuel as the present computations, the 1500 K point was shown to be in a range between 25 and 50 microns from the wall at the wall temperature of 400 K when it came closest. It is seen in Fig. 3 that the 1500 K point or quench distance at the wall temperature of 400 K is within this range.

Figure 4 shows the burning rates computed at

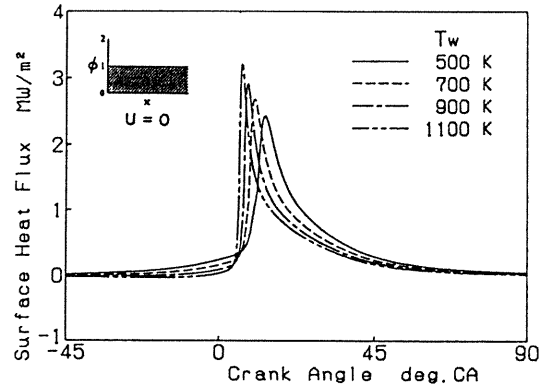

Fig. 2 Heat fluxes at different wall temperatures, for the fuel distribution A and U=0

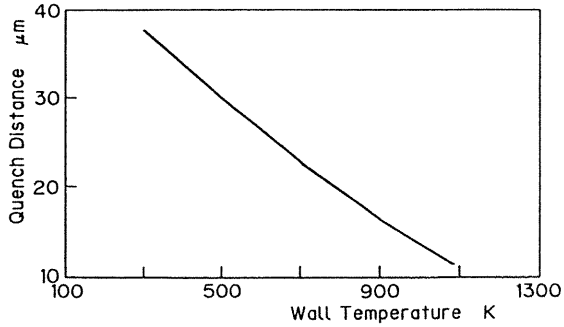

Fig. 3 Quench distance versus wall temperature for the fuel distribution A and U=0

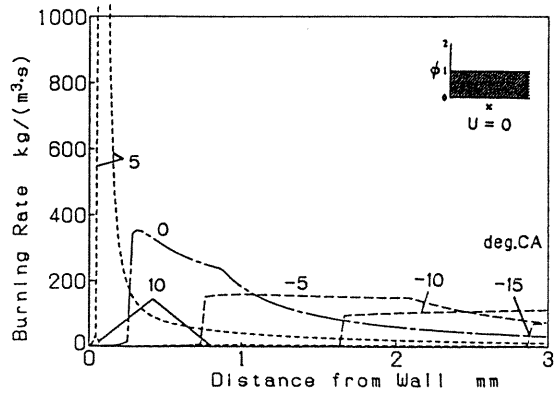

Fig. 4 Burning rate at several different crank angles for the fuel distribution A, U=0 and wall temperature Tw=1100 K.

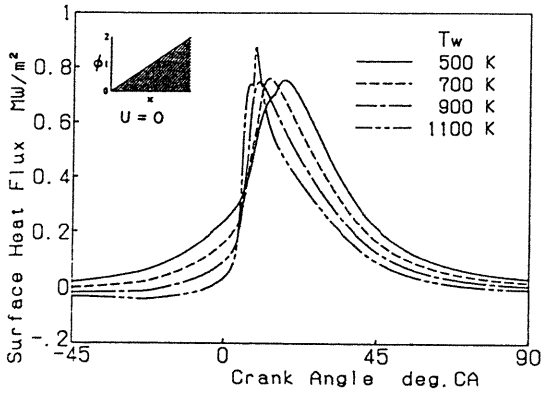

Fig. 5 Heat fluxes at different wall temperatures for the fuel distribution B and U=0

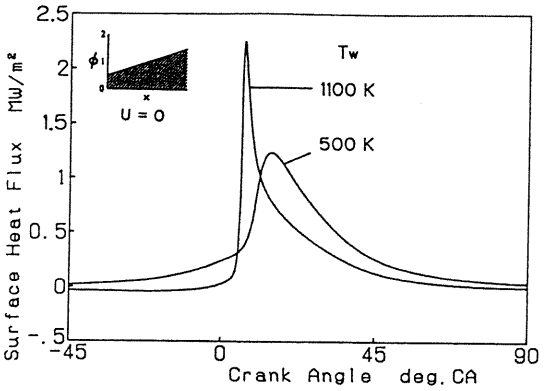

Fig. 6 Heat fluxes at different wall temperatures for the fuel distribution C and U=0

several different crank angles for the wall temperature of 1100 K. It seen that the peak value becomes higher as the flame approaches the wall. At 5 deg. CA, the burning rate exhibits an extremely high value with narrow spatial distribution close to the wall. Most part of the heat release are still controlled by the turbulent mixing at this time and the time scale becomes shorter affected by the molecular viscosity. Thus the strong heat release at the last stage of flame propagation makes the heat flux reach its peak.

Figure 5 shows heat fluxes computed for the fuel distribution B. The peak values of heat flux are seen to be much lower than those in Fig. 3, and there are not large differences among them. The reason for these behaviors can be explained as follows: the lean mixture in the near wall region makes the quench distance longer and hence has a little effect on heat fluxes to increase at higher wall temperatures; then the effect of reducing heat flux due to less temperature difference between the wall and core gas cancels the former.

The heat fluxes computed for the fuel distribution C are shown in Fig. 6. The same tendency is seen as in the case of the fuel distribution A (Fig. 3). The only difference is that the peak values are intermediate between those in the cases of the fuel distribution A and B.

HEAT FLUXES AFFECTED BY GAS MOTION APPROACHING THE WALL

In the above calculations a gas motion was represented by the velocity, u, which only

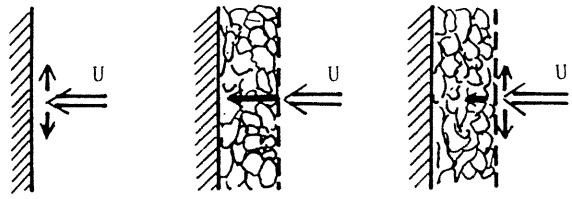

Fig. 7 Schematic of models for additional flow

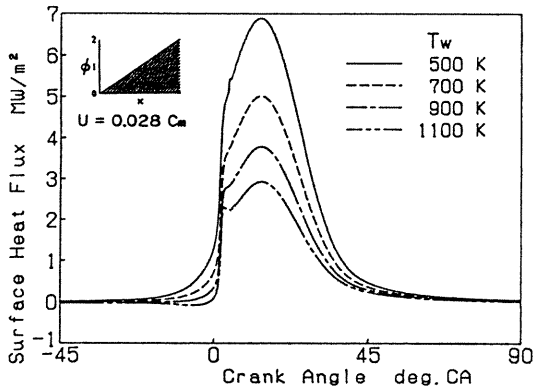

Fig. 8 Heat fluxes at different wall temperatures for the fuel distribution B and U=0.028 Cm

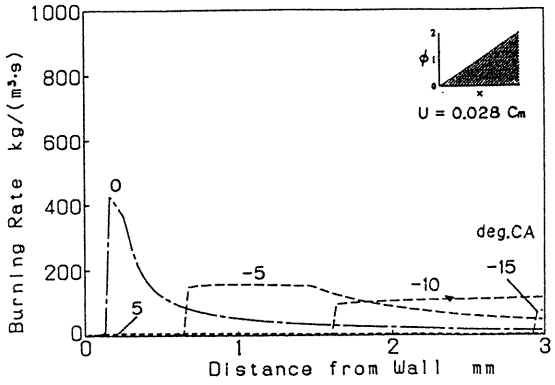

Fig. 9 Burning rate at several different crank angles for the fuel distribution B and U=0.028 Cm

reflects the compression or expansion according to the continuity equation having the boundary condition of u=0 at the wall. However, there are some possible cases where air-fuel mixtures are carried by additional gas motions approaching the wall. For example, a fuel injection may cause the additional gas motion; when a porous wall such as a plasma-sprayed-zirconia is used, the gas may penetrate into pores. To take these cases into account, an additional flow with a constant velocity, U, is added to the velocity, u, during the combustion period (from -25 to 45 deg. CA). Figure 7 schematically shows the boundary condition at the wall; the gas, which reaches the wall, either is expelled out in the direction parallel to the wall for a solid wall case, or penetrates into pores for the case of a porous wall, including an intermediate condition combining these two cases. In any case of these, the boundary condition makes no difference in the one-dimensional expression.

Figure 8 shows the heat fluxes computed for the fuel distribution B with an additional veloc-

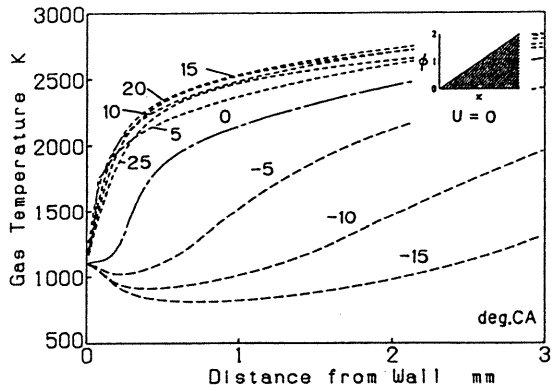

Fig. 10 Gas temperature distributions for the fuel distribution B and wall temperature Tw=1100 K without additional flow

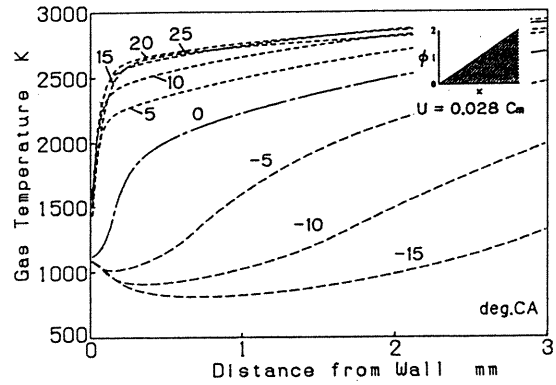

Fig. 11 Gas temperature distributions for the fuel distribution B and wall temperature Tw=1100 K with additional flow of U=0.028 Cm

ity of U=0.028 Cm, where Cm is a mean piston speed. The additional flow carries a gas in a distance of 0.35 mm during the period between the ignition and flame arrival. Supposing a porous zirconia with a thickness of 1 mm and with a porosity of 0.5, one may estimate that a gas with a thickness of 0.36 mm is compressed into the pores in the zirconia layer during the same period with the assumption of an isothermal process under the pressure shown in Fig. 1. It is noted in the figure that the heat flux decreases with increasing wall temperature; the same tendency as observed in non-reactive thermal boundary layers. Investigation of the burning rate, which is shown in Fig. 9, reveals that the heat release already ends at 5 deg. CA, while the heat flux is still increasing. Figures 10 and 11 show the temperature distributions for the cases of U=0 and U=0.028 Cm, respectively, at the wall temperature of 1100 K. Comparing the temperature distributions in these figures one may see that the additional flow carries the hot combustion products towards the wall and makes the temperature gradient near the wall even steeper after the flame arrival.

Fig. 12 shows the heat fluxes computed for the fuel distribution C with U=0.007 Cm. The heat flux curves are seen different in shape from the those in Fig. 8, but the same tendency is observed as the wall temperature is elevated. It may be estimated that the gas moves only in a distance of 0.09 mm from the ignition time to the time of flame arrival. Figure 13 shows the heat fluxes

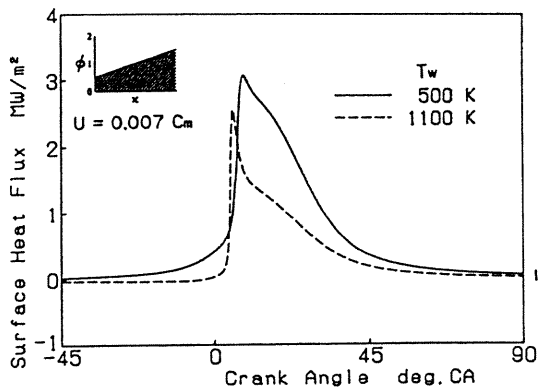

Fig. 12 Heat Fluxes at Tw=500 K and Tw=1100 K for the fuel distribution C and U=0.007 Cm

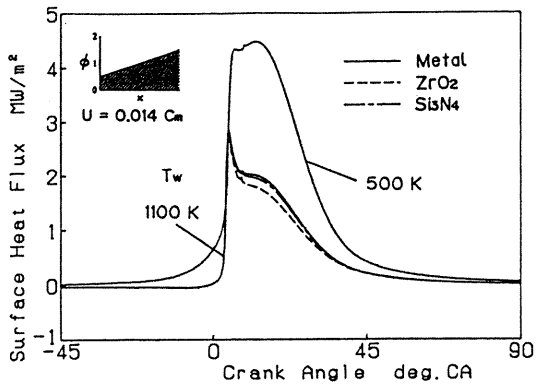

Fig. 13 Heat fluxes at Tw=500 K and Tw=1100 K for the fuel distribution C and U=0.014 Cm

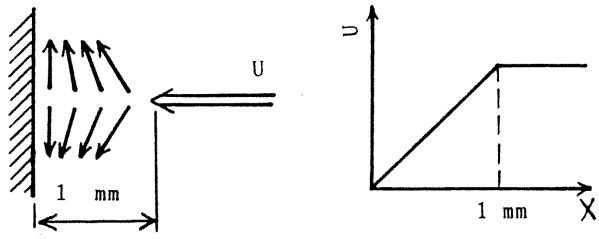

Fig. 14 Schematic of a model for additional flow turning aside in a near wall region

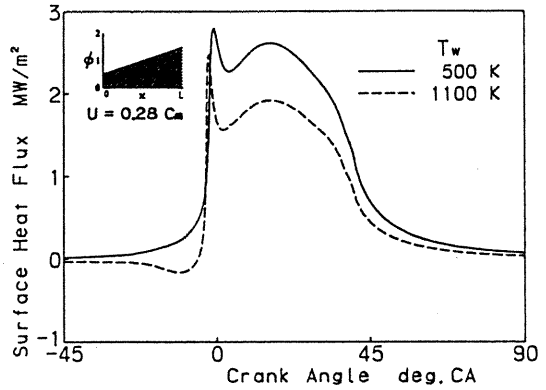

Fig. 15 Heat fluxes at Tw=500 K and Tw=1100 K for the fuel distribution C with additional flow turning aside in a near wall region

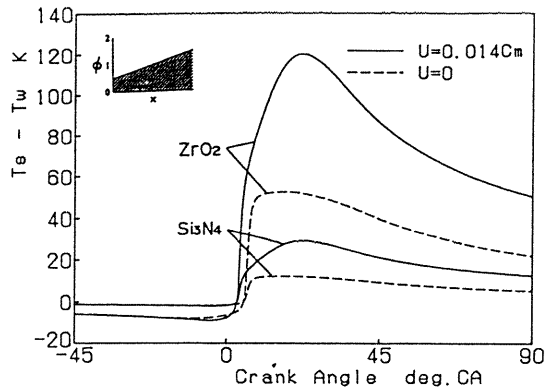

Fig. 16 Surface temperature fluctuations of ceramic walls for the fuel distribution C without and with additional flow (type shown in Fig. 7)

computed for the same conditions but U=0.014 Cm. It is seen that a stronger additional flow gives higher heat flux.

A different type of the additional flow was assumed as schematically shown in Fig. 14; the flow turns aside when it comes within 1 mm from the wall. This assumption would be more realistic for modeling a fuel spray which impinges on a solid wall. Computations were carried out for the fuel distribution C with U=0.28 Cm. The computed heat fluxes are shown in Figs. 15. In spite of much stronger additional flow, the heat fluxes are seen to be lower than those of Fig. 13. This is due to the fact that a part of the hot combustion products is expelled out when the flame front comes in the near wall region.

EFFECTS OF TEMPERATURE FLUCTUATIONS AT THE WALL SURFACE

A temperature swing at a ceramic wall surface is much larger than at a metal wall surface due to a large difference in thermal properties between them (4,5). Computations were carried out to see if the temperature fluctuations has a significant influence on wall heat fluxes. The equation for one-dimensional unsteady conduction in a solid was added and simultaneously solved along with the equations in a gas. For the computations, a plasma-sprayed-zirconia (ZrO_2) and silicon-nitride (Si_3O_4) were taken as typical examples. Heat conductivities and thermal diffusivity are 0.6 W/(m.K) and 0.545×10^{-6} m^2/s, respectively, for a zirconia; 7.5 W/(m.K) and 4.23×10^{-6} m^2/s, respectively, for a silicon nitride. Since the temperature swings were estimated to almost disappear at the depths of 0.8 mm and 1.6 mm for the zirconia and silicon nitride, respectively, a constant time-average temperature of 1100 K was given at these depths. The case of the fuel distribution C was studied for U=0 and the additional flow having U=0.014 Cm in the type of Fig. 7. The temperature fluctuations are shown in Fig. 16. It is seen that the temperature swings are considerably lower in the case of U=0 than U=0.014 Cm. Due to this, the temperature fluctuations give so little influence on heat fluxes in the case of U=0 that the difference can not be depicted in Fig. 6. The heat fluxes computed for U=0.014 Cm are shown in Fig. 13. The influence of the temperature fluctuations can be recognized, but it may be said insignificant.

CONCLUSIONS

From the one-dimensional numerical analyses of heat fluxes in reactive thermal boundary layers, the following findings are summarized:

(1) When a gas motion is induced only by compression or expansion and there is enough amount of fuel-air mixture in a near wall region , the wall heat flux increases with increasing wall temperature and peak values depend on an amount of fuel. This is because the quench distance becomes shorter with increasing wall temperature.

(2) An additional gas motion approaching the wall, which implies the penetration into a porous wall or the wall-impingement of a fuel spray, makes the heat flux decrease with increasing wall temperature. This is due to hot combustion products (non-reactive gas) coming close to the wall. A little movement of the gas is enough to exert a significant effect.

(3) The temperature fluctuations on a ceramic surface do not play an important role.

This study suggests that controlling fuel injection and gas motion, and possibly using porous wall materials have a potential to reduce heat losses during combustion in insulated combustion chambers.

ACKNOWLEDGMENTS

The authors wish to thank Assoc. Prof. Y. Yoshihara, Ritsumeikan University, for his invaluable help in formulating the combustion reaction simulation. This study was partially supported by Grant-in-Aid for Scientific Research on Priority Areas, " Exploration of Combustion Mechanism, " (No. 01627003) appropriated in 1988 and 1989 by the Ministry of Education, Science and Culture of Japan.

REFERENCES

1. Enomoto, Y. and Furuhama, S., SAE SP-700, pp.109-124, 1987.
2. Woschni, G., Spindler, W. and Kolesa, K., SAE 870339, 1987.
3. Woschni, G. and Spindler, W., Trans. ASME, J. Eng. Gas. Turbines and Power, Vol. 110, pp.482-502, 1988.
4. Huang, J.C. and Borman, G.L., SAE SP-700, pp.137-152, 1987.
5. Morel, T., Wahiduzzaman, S. and Fort, E.F., SAE SP-785, pp.185-196, 1989.
6. Cheng, W.K. Wong, V.W. and Gao, F., SAE SP-785, pp. 161-167, 1989.
7. Germerdonk, R. and Nguyen, N.N., Ger. Chem. Eng., Vol. 8,pp.81-86, 1985.
8. Yang, J. and Martin, J. K., SAE Paper No. 900690,1990.
9. Morel, T. and Monsour, N.N., SAE Paper No. 820040, 1982.
10. Myong, H.K. and Kasagi, N.,Trans. JSME, Vol.54,No.507, pp.3003-3009, 1988.
11. Gosman, A.D. and Harvey, P.S., SAE Paper No.820036, 1982.
12. Oguri, T. and Inaba, S., SAE Paper No.720023,1972.
13. Lucht, R.P. and Maris, M.A., SAE Paper No.870459, 1987.